Electronic Supplementary Information

High-Efficiency Pure Blue Thermally Activated Delayed Fluorescent Emitters with Preferentially Horizontal Emitting Dipole Orientation *via* a Spiro-linked Double D-A Molecular Architecture

Xuan Zeng,[ab] Kuan-Chung Pan,[c] Wei-Kai Lee,[c] Shaolong Gong,*[a] Fan Ni,[b] Xiao Xiao,[a] Weixuan Zeng,[a] Yepeng Xiang,[a] Lisi Zhan,[a] Yu Zhang,[a] Chung-Chih Wu*[c] and Chuluo Yang*[ab]

[a] Hubei Key Lab on Organic and Polymeric Optoelectronic Materials, Department of Chemistry, Wuhan University, Wuhan, 430072, People's Republic of China
E-mail: slgong@whu.edu.cn; clyang@whu.edu.cn

[b] College of Materials Science and Engineering, Shenzhen University, Shenzhen 518060, People's Republic of China.

[c] Department of Electrical Engineering, Graduate Institute of Electronics Engineering and Graduate, Institute of Photonics and Optoelectronics, National Taiwan University, Taipei 10617, Taiwan
E-mail: wucc@ntu.edu.tw

General Information

Toluene was dried by sodium-potassium alloy. The other reagents and solvents were used as received from commercial sources without further purification. ^{1}H NMR and ^{13}C NMR spectra were recorded by Bruker Advanced II (400 MHz) spectrometers and MERCURYVX300 using $CDCl_3$ as solvent and tetramethylsilane (TMS) as the internal standards. High resolution mass spectra (HRMS) were measured by Thermo Scientific

LTQ Orbitrap XL mass spectrometer. Differential scanning calorimetries (DSCs) were measured on a NETZSCH DSC 200 PC unit under argon with a heating rate of 10 ^{o}C min^{-1}. The glass transition temperatures (T_g) were calculated from the second heating scan. Thermo gravimetric analyses (TGAs) were performed on a NETZSCH STA 449C instrument under nitrogen with a heating rate of 10 ^{o}C min^{-1}. Cyclic voltammetry (CV) was measured on a CHI voltammetric analyzer at room temperature with the conventional three-electrode configuration, consisted of a platinum column working electrode, a platinum wire auxiliary electrode, and an Ag wire pseudo reference electrode. Cyclic voltammograms were recorded using tetrabutylammonium hexafluorophosphate ($TBAPF_6$) (0.1 M) dissolved in dichloromethane (5 mL) as the supporting electrolyte, and ferrocenium-ferrocene (Fc^+/Fc) as the external standard, at the scan rate of 100 mV s^{-1}. The onset potential was determined from the intersection of two tangents of the rising and background current in cyclic voltammogram. The geometries and FMOs were obtained by B3LYP density functional method with basis set 6-31G(d), the excited states of target molecules on ground state structures were calculated by TD-DFT procedure employing nonempirically tuned range-separated functionals LC-ωPBE with basis set 6-31G(d). The direction of the calculated transition dipole moments (TDMs) were extracted with the nuclear ensemble approach based on optimized S_1 state geometries according to published work.[S1] The spatial range of the volume data were calculated according to the literature method.[S2] The isodensity surface of ρ = 0.001 e/bohr^3 was generated by Marching Tetrahedra (MT) approach with the optimized ground state structure.

Synthetic routes

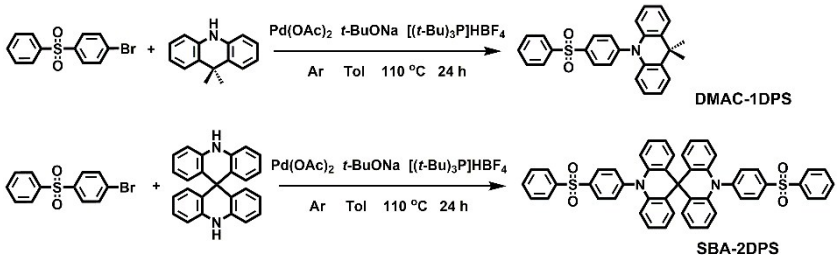

Scheme S1 Synthetic routes of the **DMAC-1DPS** and **SBA-2DPS**.

X-Ray Structural Analysis

Single crystal of **DMAC-1DPS** was obtained from slow evaporation of cyclohexane/$CHCl_3$ solution at room temperature, its X-ray-diffraction data was obtained from a Bruker APEX2 Smart CCD diffractometer through using MoKα radiation (λ = 0.71073 Å) with a $\omega/2\theta$ scan mode at the temperature of 296 K. crystal structure of the **DMAC-1DPS** was solved by direct methods using the SHELXL-2014/7′ software. None-hydrogen atoms were refined anisotropically by full-matrix least-squares calculations on F^2 using SHELXL-2014/7′, while the hydrogen atoms were directly introduced at calculated position and refined in the riding mode. With respect to **SBA-2DPS**, its crystal was obtained from slow evaporation of ethanol/$CHCl_3$ solution at room temperature, the X-ray-diffraction data was collected at 100 K on a Rigaku Oxford Diffraction Supernova Dual Source, Cu at Zero equipped with an AtlasS2 CCD using Cu Kα radiation (λ = 1.54184 Å). Crystal structure of the **SBA-2DPS** was solved by direct methods using the SHELXL-2018/3′ software. None-hydrogen atoms were refined anisotropically by full-matrix least-squares calculations on F^2 using SHELXL-2018/3′, while the hydrogen atoms were directly introduced at

calculated position and refined in the riding mode. Drawings were produced using Mercury-3.3. CCDC-1868668 (**DMAC-1DPS**) and CCDC-1868667 (**SBA-2DPS**) contain supplementary crystallographic data. These data can be obtained free of charge from the Cambridge Crystallographic Data Centre *via* www.ccdc.cam.ac.uk/data_request/cif.

Photophysical Characterization

Thin films for photophysical characterization were prepared by thermal evaporation on quartz substrates at 1-2 Å/sec in a vacuum chamber with a base pressure of $<10^{-6}$. torr. UV-vis absorption spectra were performed on a Shimadzu UV-2700 spectrophotometer. Photoluminescence (PL) spectra, photoluminescence quantum yields (Φ_{PL}s), and phosphorescence spectra were characterized by a spectrofluorimeter (FluoroMax-P, Horiba Jobin Yvon Inc. or F-4600, Hitachi Inc.). Φ_{PL}s of thin films were determined under dry nitrogen environment using these spectrofluorimeters equipped with a calibrated integrating sphere. The transient photoluminescence decay curves were measured by a single photo counting spectrometer from Edinburgh Instruments (FLS920) using a picosecond pulsed UV-LASTER (LASTER377) as the excitation source.

Determination of the emitting dipole orientation of an emitting layer:

To determine the emitting dipole orientation in a molecular emitting film, angle-resolved and polarization resolved PL measurements were performed. The sample consisted of a fused silica substrate with the 20-nm-thick DPEPO film doped with emitters. The sample was attached to a fused silica half cylinder prism by index

matching liquid. The excitation of the samples was performed with the 325-nm line of the continuous-wave He:Cd laser with a fixed excitation angle of 45°. The emission angle was changed by use of an automatic rotation stage. The spectra were resolved by using a p-polarizing filter and were measured by a fiber optical spectrometer. The angle-dependent p-polarized emission intensity at the peak wavelength of the PL spectrum of the emitting layer was detected. The emitting dipole orientation (the horizontal dipole ratio $\Theta_{//}$) was then determined by least square fitting of the measured angle-dependent p-polarized emission intensity with calculated results.

Device fabrication and measurement:

All organic materials used in experiments (except for the TADF emitters) were purchased from Lumtec, Inc. All compounds were subjected to temperature-gradient sublimation under high vacuum before use. OLEDs were fabricated on the ITO-coated glass substrates with multiple organic layers sandwiched between the transparent bottom indium-tin-oxide (ITO) anode and the top metal cathode. All material layers were deposited by vacuum evaporation in a vacuum chamber with a base pressure of 10^{-6} torr. The deposition system permits the fabrication of the complete device structure in a single vacuum pump-down without breaking vacuum. The deposition rate of organic layers was kept at 0.1-0.2 nm/s. The doping was conducted by co-evaporation from separate evaporation sources with different evaporation rates. The active area of the device is 1×1 mm^2, as defined by the shadow mask for cathode deposition. The current-voltage-brightness (J-V-L) characterization of the light-emitting devices was performed with a source-measurement unit (SMU) and a spectroradiometer (DMS 201,

AUTRONIC-MELCHERS GmbH). The EL spectra were measured by a calibrated goniometric spectroradiometer (DMS 201, AUTRONIC-MELCHERS GmbH). The external quantum efficiencies of devices were determined by collecting the total emission fluxes with a calibrated integrating-sphere measurement system and by measuring the angular distribution of the emission spectra and intensities.

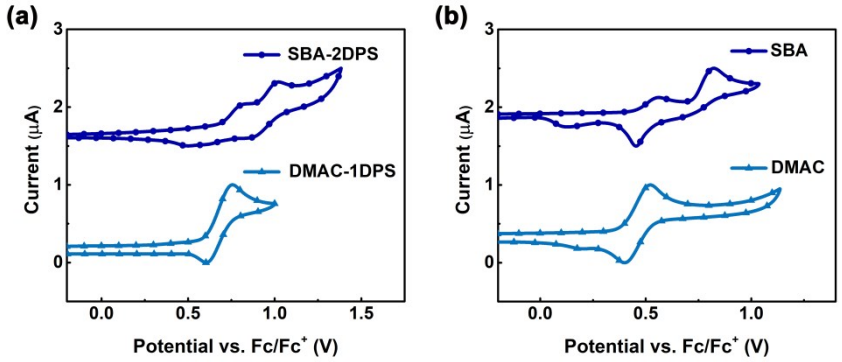

Fig. S1 Cyclic voltammograms of (a) emitters and (b) donor moieties measured in CH_2Cl_2.

Table S1. The summary of thermal and electrochemical properties of **DMAC-1DPS** and **SBA-2DPS**.

Compound	T_g[a)] [°C]	T_d[b)] [°C]	HOMO[c)] [eV]	LUMO[d)] [eV]	E_g[e)] [eV]
DMAC-1DPS	69	295	-5.40	-2.34	3.06
SBA-2DPS	176	476	-5.49	-2.42	3.07

[a)]Measured by DSC; [b)]Measured by TGA; [c)]Obtained from cyclic voltammograms in CH_2Cl_2 solution at room temperature; [d)]LUMO = HOMO - E_g[e]; [e)]Energy gap (E_g) obtained from the intersection of the normalized absorption spectra.

Analyses of Rate Constants:

According to previous reports, the rate constants were calculated by assuming that most of triplet states can return to singlet states through reverse intersystem crossing (RISC) and major nonradiative losses occur in singlet states.[S3]

$$k_p = \frac{1}{\tau_p} \quad \text{Ⅰ}$$

$$k_d = \frac{1}{\tau_d} \quad \text{Ⅱ}$$

$$k_{r,S} = \Phi_{PF} k_p + \Phi_{DF} k_d \approx \Phi_{PF} k_p \quad \text{Ⅲ}$$

$$k_{nr,S} = \frac{1 - \Phi_{PL}}{\Phi_{PL}} k_{r,S} \quad \text{Ⅳ}$$

$$k_{ISC} \approx \frac{k_p k_d \Phi_{DF}}{k_{RISC} \Phi_{PF}} \quad \text{Ⅴ}$$

$$k_{RISC} \approx \frac{k_p k_d \Phi_{PL}}{k_{r,S}} \quad \text{Ⅵ}$$

$$\Phi_{ISC} = \frac{k_{ISC}}{k_{r,S} + k_{ISC} + k_{nr,S}} \quad \text{Ⅶ}$$

where τ_p and τ_d are lifetime of the prompt and delayed component in transient PL curves, Φ_{PL}, Φ_{PF} and Φ_{DF} are total photoluminescence quantum yield, quantum yield for the prompt fluorescence and quantum yield for the delayed fluorescence, respectively. The detail data were summarized as below.

Table S2. The summary of rate constants for emitters in doped DPEPO films.

Compound	$k_{r,S}$[a] [10^7 s^{-1}]	$k_{nr,S}$[b] [10^6 s^{-1}]	k_p[c] [10^7 s^{-1}]	k_d[d] [10^5 s^{-1}]	k_{ISC}[e] [10^7 s^{-1}]	k_{RISC}[f] [10^5 s^{-1}]	Φ_{ISC}[g]
DMAC-1DPS	0.97	6.17	4.90	2.38	3.27	7.37	0.67
SBA-2DPS	1.37	9.11	5.26	2.33	2.96	5.38	0.56

[a]Radiative decay rate from the S_1 state; [b]Nonradiative decay rate from the S_1 state; [c]Decay rate constants for prompt fluorescence; [d]Decay rate constants for delayed fluorescence; [e]Intersystem crossing rate; [f]Reverse intersystem crossing rate; [g]Quantum efficiency of intersystem crossing.

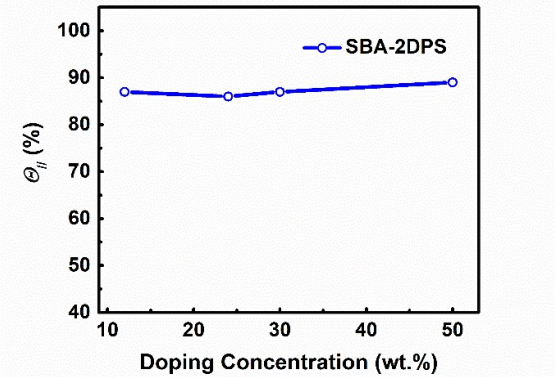

Fig. S2 Horizontal dipole ratios ($\Theta_{//}$) of the **SBA-2DPS** as a function of the doping concentration.

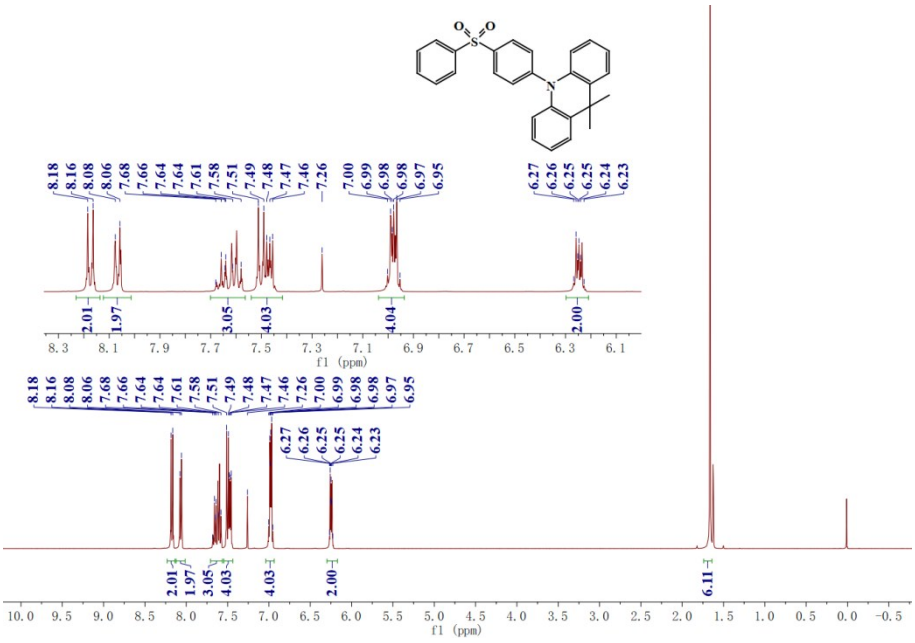

Fig. S3 ^{1}H NMR spectra of **DMAC-1DPS** (400 MHz, $CDCl_3$ + TMS, 25 ^{o}C).

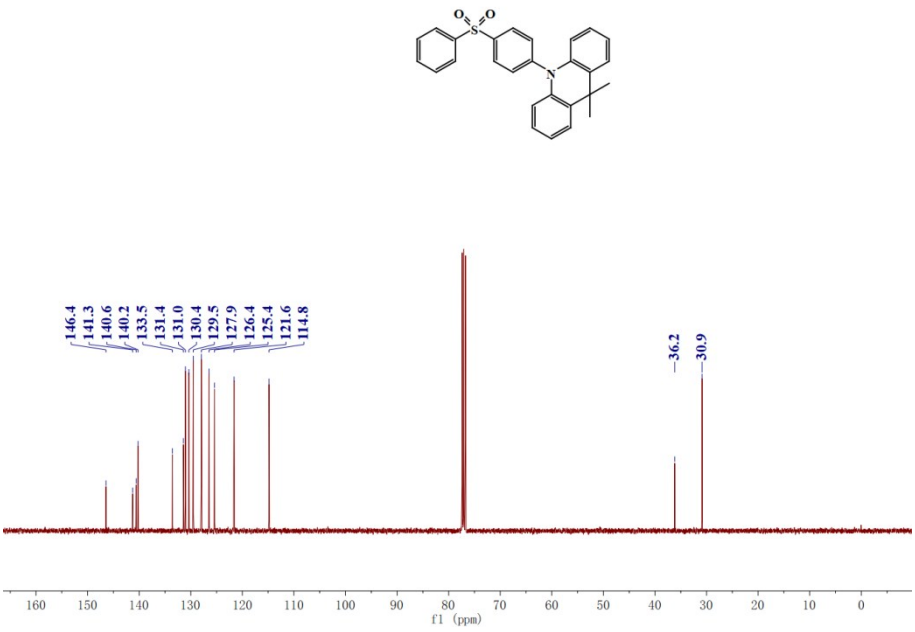

Fig. S4 ^{13}C NMR spectra of **DMAC-1DPS** (100 MHz, $CDCl_3$ + TMS, 25 ^{o}C).

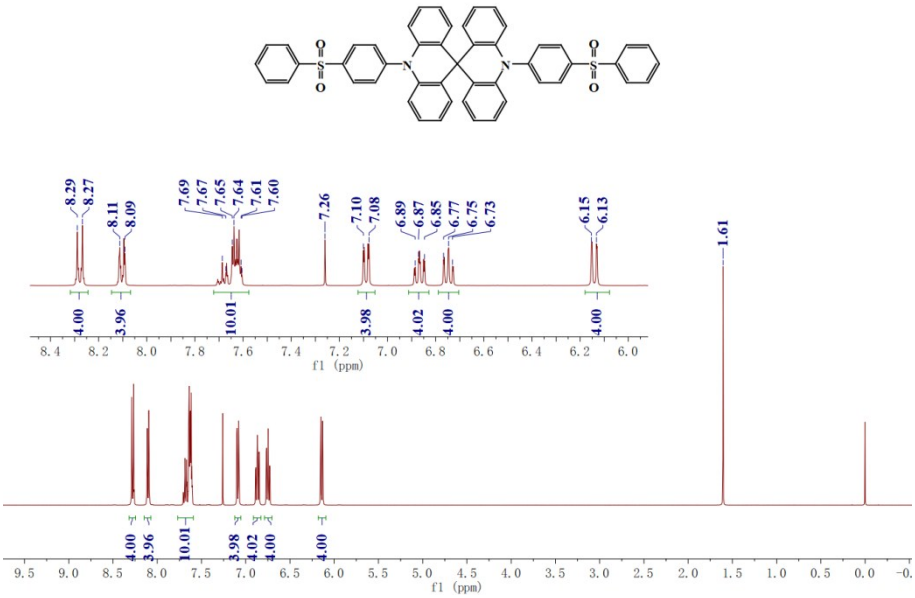

Fig. S5 ^{1}H NMR spectra of **SBA-2DPS** (400 MHz, $CDCl_3$ + TMS, 25 ^{o}C).

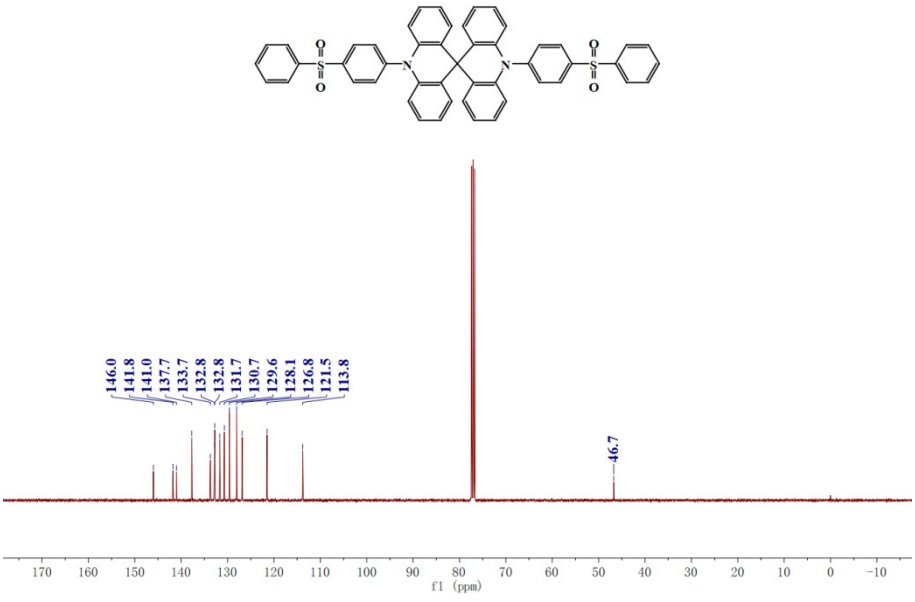

Fig. S6 ^{13}C NMR spectra of **SBA-2DPS** (100 MHz, $CDCl_3$ + TMS, 25 ^{o}C).

References

S1 W. Zeng, S. Gong, C. Zhong and C. Yang, *J. Phys. Chem. C*, 2019, **123**, 10081-10086.

S2 T. Lu and F. Chen, *J. Mol. Graph. Model.*, 2012, **38**, 314-323.

S3 K.-C. Pan, S.-W. Li, Y.-Y. Ho, Y.-J. Shiu, W.-L. Tsai, M. Jiao, W.-K. Lee, C.-C. Wu, C.-L. Chung, T. Chatterjee, Y.-S. Li, K.-T. Wong, H.-C. Hu, C.-C. Chen and M.-T. Lee, *Adv. Funct. Mater.*, 2016, **26**, 7560-7571.